# Persistent westward drift of the geomagnetic field at the core-mantle boundary linked to recurrent high latitude weak/reverse flux patches

Andreas Nilsson[1]*, Neil Suttie[1], Monika Korte[2], Richard Holme[3], Mimi Hill[3]

[1] Department of Geology, Lund University, Sweden

[2] GFZ German Research Centre for Geosciences, Potsdam, Germany

[3] Department of Earth, Ocean and Ecological Sciences, University of Liverpool, Liverpool, UK

*Corresponding author: e-mail: andreas.nilsson@geol.lu.se, phone: +46 46 2223952.

Abbreviated title: “Westward drift linked to high latitude weak/reverse flux”.

## Abstract

Observations of changes in the geomagnetic field provide unique information about processes in the outer core where the field is generated. Recent geomagnetic field reconstructions based on palaeomagnetic data show persistent westward drift at high northern latitudes at the core-mantle boundary (CMB) over the past 4000 years, as well as intermittent occurrence of high latitude weak or reverse flux patches. To further investigate these features we analysed time-longitude plots of a processed version of the geomagnetic field model pfm9k.1a, filtered to remove quasi-stationary features of the field. Our results suggest that westward drift at both high northern and southern latitudes of the CMB have been a persistent feature of the field over the past 9000 years. In the northern hemisphere we detect two distinct signals with drift rates of 0.09°/year and 0.25°/year and dominant zonal wavenumbers of $m$ = 2 and $m$ = 1 respectively. Comparisons with other geomagnetic field models support these observations but also highlight the importance of sedimentary data that provide crucial information on high latitude geomagnetic field variations. The two distinct drift signals detected in the northern hemisphere can largely be decomposed into two westward propagating waveforms. We show that constructive interference between these two waveforms accurately predicts both the location and timing of previously observed high latitude weak/reverse flux patches over the past three to four millennia. In addition, we also show that the 1125-year periodicity signal inferred from the waveform interference correlates positively with variations in the dipole tilt over the same time period. The two identified drift signals may partially be explained by the westward motion of high latitude convection rolls. However, the dispersion relation might also imply that part of the drift signal could be caused by magnetic Rossby waves riding on the mean background flow.

Keywords: Palaeomagnetism; Palaeomagnetic secular variation; Core; Magnetic field variations through time

## 1. Introduction

Earth's magnetic field is believed to be generated by convection in Earth's iron-rich liquid outer core, a process known as the geodynamo. Observed changes of the geomagnetic field, also known as secular variation, have the potential to constrain the processes responsible for maintaining it. As early as the 17$^{th}$ century, Halley (1692) noted that specific features of the geomagnetic field at Earth's surface appear to drift predominantly in a westward direction. By calculating the drift rate around latitudinal circles, Bullard *et al.* (1950) inferred a global average rate of 0.18°/year for the westward drift of the non-dipolar field at Earth's surface over the period 1907 - 1945.

With the development of geomagnetic field models designed to map the field at the core-mantle boundary (CMB), Bloxham and Gubbins (1985) established that the westward drift is not a global phenomenon but mainly restricted to the region between 90°E and 90°W. By studying the non-axisymmetric flux at the core, Finlay and Jackson (2003) showed that the observed drift is most prominent in the equatorial region, with westward motion of flux at a rate of 17 km/year (equivalent to 0.27°/year) persisting throughout the past four centuries. Westward drift is also observed at high latitudes, with (south)west movement of an intense flux patch beneath Patagonia over the same time period and more recently the accelerated westward motion (up to 0.90°/year) of an intense flux patch beneath Canada, potentially associated with a high-latitude jet (Livermore *et al.*, 2017). All of these observations are consistent with, or can at least partially be explained by, a giant westward drifting eccentric planetary gyre (Barrois *et al.*, 2018), originally isolated in core flow inversions by Pais and Jault (2008). This planetary gyre has been successfully reproduced in numerical dynamo simulations involving both gravitational coupling of the inner core to the mantle and differential inner core growth causing preferential buoyancy release in the outer core beneath the Indian Ocean (Aubert *et al.*, 2013).

An alternative hypothesis for the observed westward drift, originally proposed by Hide (1966), involves the propagation of magnetohydrodynamic waves. According to this theory the horizontal velocity of the fluid is not necessarily the same as the westward drift velocity. Rotating magnetic-Coriolis waves are split into two classes, fast 'inertial' modes and slow 'magnetic' modes, with the latter operating on timescales of 100-10,000 years (Finlay et al., 2010). Hide (1966) investigated a specific quasi-geostrophic (i.e. with little variation in the z-direction) form of the slow magnetic-Coriolis waves, often called magnetic Rossby waves, which he found were likely to contribute to secular variation. These waves propagate westwards and are dispersive (shorter wavelengths have

faster phase velocities). Hori et al. (2015; 2018) recently demonstrated that westward drifts in dynamo simulations, similar to those observed over the past four centuries, could be explained by such magnetic Rossby waves riding on mean flow advection. Various excitation mechanisms have been proposed that could produce these waves, including turbulence in the core (Hide, 1966), topographic differences at the CMB (Hide, 1966) or even length-of-day (LOD) variations through topographic core-mantle coupling (Yoshida and Hamano, 1993).

Investigations of azimuthal motions in geomagnetic field models constrained by palaeomagnetic data have shown evidence for both eastward and westward drift (Dumberry and Finlay, 2007, Wardinski and Korte, 2008, Amit *et al.*, 2011, Nilsson *et al.*, 2014, Hellio and Gillet, 2018). The azimuthal motions in the field are most clearly seen at mid- to high northern latitudes, linked to movements of intense flux patches at the CMB (Dumberry and Finlay, 2007), which is likely a reflection of structures that can be resolved by these models. Based on the (now superseded) CALS7K.2 model, Dumberry and Finlay (2007) and Wardinski and Korte (2008) observed more or less equal occurrence of eastward and westward drift, with typical drift rates of ±0.15°/year at 40-60°N. Amit et al. (2011) based their analysis on the CALS3K.3 model (Korte *et al.*, 2009), using an algorithm to identify and track movements of intense (normal polarity) flux patches found mostly around the edge of the inner core tangent cylinder. They also observed both eastward and westward motions with average drift rates around 0.20°/year, although westward drift was slightly more common. Studies based on more recent geomagnetic field reconstructions (Nilsson *et al.*, 2014, Hellio and Gillet, 2018), however, show a clear dominance of westward drift over the past 4000 years with drift rates of 0.20 – 0.25°/year reported by Hellio and Gillet (2018) and persistent slow drift rates of ~0.07°/year (equivalent to a 5000 year rotation period) reported by Nilsson *et al.* (2014).

In addition to persistent westward drift, Nilsson *et al.* (2014) also noted the intermittent occurrence (1500BC, 300BC, 700AD, 1900AD) of weak or reversed flux patches at high northern latitudes at the CMB, potentially originating at low latitudes and migrating polewards. Campuzano *et al.* (2019) described in more detail the evolution of the most recent of these high latitude weak/reverse flux patches. They find that the flux patch emerged at the equator in the Atlantic hemisphere around 1000-1400 AD and moved north-eastward at a rate of 10 km/year. They further note that the evolution of this flux patch was more or less antisymmetric to the simultaneous south-westward migration of another reverse flux patch associated with the development of the South Atlantic Anomaly (SAA), suggesting that these observations could be linked. However, similar hemispherical asymmetries have not been observed for the other occurrences of high latitude weak/reverse flux.

Attempts have also been made to identify and track movements of reverse flux patches. Based on the method of Amit et al. (2011), Terra-Nova *et al.* (2015) noted that reverse flux patches mostly

exhibit westward drift and generally migrate toward higher latitudes. Terra-Nova *et al.* (2015) also concluded that the detection of reverse flux patches is strongly dependent on spherical harmonic degrees 4 and above, which is at the limit of what current palaeomagnetic field models can robustly resolve, particularly in the southern hemisphere of the core (Nilsson *et al.*, 2014).

Overall, the observations of azimuthal motions and reverse flux patches in the palaeomagnetic record vary significantly between different studies. The discrepancies can largely be explained by differences between the geomagnetic field models (many of which are now superseded) rather than the methods used to analyse the data (e.g. Terra-Nova *et al.*, 2016). A range of new millennial scale geomagnetic field models has been produced over the past few years (Nilsson *et al.*, 2014, Pavón-Carrasco *et al.*, 2014, Hellio and Gillet, 2018, Constable *et al.*, 2016, Campuzano *et al.*, 2019, Arneitz *et al.*, 2019). These models are based on more or less the same data compilation, which has been vastly improved from the earliest versions, e.g. used to constrain CALS7K.2 (Korte *et al.*, 2005). This data compilation typically includes archaeomagnetic data from GEOMAGIA50.v3 database (Brown *et al.*, 2015), which is continually updated, and in some cases sedimentary data compiled by Korte *et al.* (2011) and later augmented by Panovska *et al.* (2015). Overall the agreement between the different palaeomagnetic field models has improved, but significant differences still exist. The most important difference between these models can be traced to the choices of how to treat sedimentary data, which if included will improve data coverage while also leading to smoother models, e.g. due to post-depositional processes (Nilsson *et al.*, 2018). Different strategies of how to address data uncertainties and outliers and how much weight is given to different data types (e.g. sedimentary data) also have potentially large impacts on the resulting models.

The main objective of this study is to investigate the persistence of westward drift at the CMB on Holocene timescales and whether or not this is linked to the occurrence of reverse flux at high northern latitudes. The analyses will primarily be based on the pfm9k.1a model, which uses a crude Bayesian approach to synchronize timescales of different sediment records based on the palaeomagnetic data (Nilsson *et al.*, 2014). To evaluate how robust our observations are, we compare our results with similar analyses on models constructed using different modelling strategies and data as well as different models from the same model family.

## 2. Methods

### *2.1 Time-longitude plots*

To investigate eastward and westward drift we use so-called time-longitude (TL) plots, calculated with a 2° and 10-year grid size, and follow the approach of Finlay and Jackson (2003) and Dumberry

and Finlay (2007). First we remove the time-averaged axisymmetric part of the field and then high-pass filter the Gauss coefficients with a cut-off frequency of 1/2500 years$^{-1}$. The cut-off frequency, similar to 1/2000 years$^{-1}$ used by Dumberry and Finlay (2007), was found to be enough to filter out quasi-stationary field structures without removing too much of the original signal. We estimate that the residual field captures 52% of the variability of the original radial field ($B_r$) at the core mantle boundary (CMB) (see supplementary material). The filtered model is given the suffix '_p' to distinguish it from the original model. To avoid end-effects related to the zero-phase Butterworth filter we remove 300 years at the beginning and end of the model. Although pfm9k.1a model covers the time period 7500 BC to 2000 AD, it was only intended to be used for the period 7000 BC to 1900 AD and we therefore restrict our analyses to the to the period 7000 BC to 1700 AD.

*2.2. Radon drift determination*

To quantitatively estimate the azimuthal drift rates observed in the time-longitude plots we use a technique based on Radon transform (for more details see, Dumberry and Finlay, 2007, Finlay and Jackson, 2003). The Radon transform of a 2D TL image provides a measure of the amount of coherent signal found along different angles of the image, which directly translates to different azimuthal drift rates. In addition to Radon drift determinations of TL plots at latitudes from 70°S to 70°N, we calculated drift rates based on Radon transforms for pfm9k.1a_p at 60°N over 2500-year moving windows at 100-year time steps. The resulting so-called time-drift plots, with the signal power in each window normalised to the maximum value, are useful to investigate the persistence over time of observed high latitude westward drift.

*2.3 Frequency–wavenumber analysis*

To further investigate the identified drift rates, we use two-dimensional frequency-wavenumber power spectra of the TL plots at 60°N, where the strongest drifts occur, which were calculated using fast Fourier transform. Peaks in these power spectra identify dominant zonal wavenumbers $m$ = 360°/$\lambda$ (where $\lambda$ is the angular wavelength) and frequencies $f = 1/T$ (where $T$ is the period in years). Based on the time-drift plots from the Radon transform we calculated the frequency-wavenumber power spectra for three partially overlapping time-windows; 2000BC – 1700AD, 5000BC – 1000BC and 7000BC – 4000BC. In the following, unless explicitly specified, we adopt the convention of expressing frequencies and drift rates as negative (positive) for westward (eastward) propagation directions.

## 3. Results

### *3.1 Analysis of the past 9000 years from the pfm9k.1a model*

Time-longitude plots at 60°N, of the original model (pfm9k.1a) and filtered model (pfm9k.1a_p) are shown in Figure 1. We chose 60°N as this is where the high latitude intense flux patches are mainly seen and, as we will see from the Radon transform results, also where the strongest azimuthal drift rates are observed. The time-longitude plots show mostly evidence for westward drift, manifested as diagonal lines going from the bottom right to top left. Eastward drift is also observed (e.g. around 2000–1000BC; -90–0°E), but these features appear to be less continuous in time. The filtered version (Fig. 1b) shows drift signatures much more clearly, so we focus on that in the following. Moreover, to better illustrate slow drift we extend the longitudinal range to -360° - 360°, i.e. showing two duplicate time-longitude plots next to each other in that panel.

We distinguish at least two different westward drift rates, (i) a slow -0.09°/year (corresponding to 2.7 km/year) drift superimposed by a (ii) faster -0.25°/year (7.6 km/year) propagating signal, marked by the dash-dot and dashed lines respectively in the figure. The slow westward drift rate is similar to the -0.07°/year drift (corresponding to a 5000-year rotation period) previously noted by Nilsson et al., (2014) over the past 4000 years. However, after high-pass filtering the model we find evidence that this slow westward drift has been persistent throughout the past 9000 years. The faster drift rate is consistent with classic westward drift originally proposed by Bullard (1950) and recently noted by Hellio and Gillet (2018) in their model COV-LAKE covering similar timescales.

The lines in Figure 1b (and Fig. 1a) have deliberately been plotted along transects of positive residual field (corresponding to weak or reverse flux in the unfiltered model; Fig. 1a) where the drift signal appears to be stronger. The drift lines are only continuous, indicating movement of a single flux patch, over shorter time periods. In general, the observed drift lines are rather patchy, consistent with a stop-and-go motion described by Nilsson et al. (2014) or a preferred location/configuration of flux. The faster drift signal is mostly visible in the Pacific hemisphere between 90°E and 270°E. We also note a general occurrence of more intense flux around 0, 90, 180, 270°E, suggesting the potential presence of one or two standing waves.

In Figure 2a we show the results from Radon transform of TL plots at latitudes from 70°S to 70°N for pfm9k.1a_p. As previously stated, the strongest (dominantly westward) drift rates are observed at high northern latitudes, around 60°N, with two distinct drift rates (-0.09°/year and -0.25°/year) being resolved. The analysis also reveals dominant westward drift (-0.22°/year) at high southern latitudes, around 60°S, as well as notable peaks in signal power associated with eastward drift (~0.15°/year) at northern mid-latitudes.

The results of the time-drift plots shown in Figure 2b indicate persistent westward drift at 60°N throughout the past 9000 years. There is a strong ~0.09°/year westward drift signal present for most of the record with faster westward drift rates (~0.25°/year) appearing around 3000BC and onwards. In the earliest few time windows the two signals appear to merge into a single peak around -0.20°/year.

The frequency-wavenumber spectra for the three overlapping time intervals at 60°N are shown in Figure 3a-c. For the first time window (2000 BC to 1700 AD) the power spectra show westward propagating waves with dominant zonal wavenumbers of $m$ = 1 and $m$ = 2. This is consistent with the two identified drift rates being described by an $m$ = 2 waveform ($f$ = -1/2000 year$^{-1}$ with drift rate $d$ = $\lambda f$ = -0.09°/year) and an $m$ = 1 waveform ($f$ = -1/1440 year$^{-1}$ with drift rate $d$ = $\lambda f$ = -0.25°/year) respectively (see stars in Figure 3a as well as the dashed-dotted and dashed lines in Figure 1). We also find a weak $m$ = 2 signal in eastward direction around $f$ = 1/2000 year$^{-1}$ (as well as $f$ = 1/1000 year$^{-1}$), which would be expected from the presence of a standing wave, previously mentioned.

From 5000 to 1000 BC the $m$ = 1 waveform (representing the faster drift rates) is more or less absent, which is consistent with the observations from time-drift plot in Figure 2b. The weaker $m$ = 2 eastward drift signal also persists at similar frequencies. In the earliest time-window (7000 – 4000 BC) the strongest signal is found at an intermediate frequency around $f \approx$ -1/1800 year$^{-1}$ with zonal wavenumber $m$ = 1, which corresponds to the -0.20°/year drift rates observed in Figure 2b.

In Figure 3d we show the frequency-wavenumber spectrum of the TL plot at 60°S latitude over the first time window (2000 BC to 1700 AD). The strongest signal is associated with a westward propagating $m$ = 1 waveform at frequency $f \approx$ -1/1650 year$^{-1}$, which is consistent with the single peak in drift rates at high southern latitudes of -0.22°/year determined using the Radon transform method (Fig. 2a).

### *3.2 Effects of model resolution*

The resolution of pfm9k.1a at the core mantle boundary varies spatially (and temporally) due to the uneven distribution of the palaeomagnetic data used to constrain the model (e.g. more than 88% of the data come from the northern hemisphere). Based on comparisons with the *gufm1* model, Nilsson *et al.* (2014) estimated that the pfm9k.1a model resolution at 1900AD is roughly equivalent to a spherical harmonic truncation at degree 5-6 in the northern hemisphere and degree 3-4 in the southern hemisphere. These truncation levels could probably be regarded as upper limits for the full 9000-year range of the model. The low model resolution at high southern latitudes limits the waveform structures we can expect to resolve in this region but could also lead to a distortion of the signal due to aliasing effects.

To demonstrate this we performed the same analyses as in section 3.1 on a low-resolution version of the pfm9k.1a model, truncated at spherical harmonic degree 4 (pfm9k.1a[$l_{max}$=4]). In Figure 4a and 4b, respectively, we show the results of both the Radon drift determination (7000BC – 1700AD) and the frequency-wavenumber spectrum of the TL plot at 60°N (2000 BC to 1700 AD) based on the truncated pfm9k.1a, filtered in the same way as the original model. The Radon drift determination of the truncated model (Fig. 4a) fails to distinguish the two drift rates at high northern latitudes (Fig. 2a) and instead only shows a single peak. Similar to our observations for 60°S in the original model, the truncated model does not show any *m* = 2 structures at 60°N but instead shows a broad peak at zonal wavenumber *m* = 1 covering the frequency range of the previously proposed waveforms (Fig. 4b).

This comparison implies that the observed differences between the northern and southern hemisphere drift signals could be explained by spatial variations in the model resolution. However, a visual comparison between the TL plots at 60°S of the original model and at 60°N of the truncated model (see supplementary material, Figure S2) also reveals that the detected signals drift in and out of phase with each other, suggesting that model resolution can only explain part of the differences. We also note that the largely comparable observations at 60°N from the early part of pfm9k.1a_p, i.e. -0.20°/year drift rates dominated by zonal wavenumbers *m* = 1 (Fig. 2b and Fig. 3c), suggest that the lack of two distinct signals in this time period could potentially also be related to limited model resolution due to the decrease in data density with increasing time. In the same way that the model resolution in the southern hemisphere limits (and potentially distorts) what we can detect we should also expect that the model resolution in the northern hemisphere probably prevents us from detecting anything beyond zonal wavenumber *m* = 2.

*3.3 Model comparison*

To investigate the robustness of our observations, so far based only on pfm9k.1a_p, we applied the Radon drift determination to different models constructed with different modelling strategies and data (Fig. 5a-d) as well as to different models within the same model family (Fig. 5e-g). Note that for COV-LAKE and COV-ARCH, which consist of ensembles of models, the suffix '_M' is added to highlight that the results are based on the mean model.

In all cases, except for COV-ARCH_M_p which is the only model that excludes sedimentary data, we find strong signals associated with the two distinct westward drift rates at high northern latitudes as identified in pfm9k.1a_p. In COV-ARCH_M_p at similar latitudes, we find a peak around -0.22°/year and only a weak signal associated with the -0.09°/year drift rates. Similarly to the southern hemisphere signal in pfm9k.1a_p, the frequency-wavenumber spectrum for COV-ARCH_M_p is

dominated by $m$ = 1 structures (see supplementary information, Figure S5). This is likely due to the lack of archaeomagnetic data at high northern latitudes, reducing the spatial resolution of the model in this region of the CMB and the ability to resolve $m$ = 2 structures (see section 3.2).

All three models that include sedimentary data show elevated drift signals at high southern latitudes. The dominance of westward drift, observed in pfm9k.1a_p, is reproduced in two models (Fig. 5b-c), with peaks around similar drift rates (-0.22°/year). We note that in these two models the observed westward drift at 60°S is associated with zonal wavenumbers $m$ = 1 (see supplementary material), similarly to pfm9k.1a_p. The absence of corresponding strong drift signals at high southern latitudes in COV-ARCH_M_p is perhaps not surprising given the general lack of archaeomagnetic data from this region. In addition to the observed high latitude westward drift, two models (Fig. 5a and 5c) also show support for eastward drift at northern mid-latitude, previously identified in pfm9k.1a_p.

To compare Radon drift determinations between models from the same model families we focus on latitude 60°N (Fig. 5e-g). Of the investigated model families there are three bootstrap models available: pfm9k.1b, COV-LAKE, COV-ARCH. It is worth noting that the pfm9k.1a model is not the same as the average model of pfm9k.1b but could rather be regarded as one of the most likely draws from this ensemble due to the synchronization of the individual sediment timescales. We find good support for the 0.09°/year westward drift signal in both pfm9k.1b and COV-LAKE but not in COV-ARCH, which is consistent with the observations from the model average. Elevated signal power around drift rates -0.25°/year are present in most of COV-LAKE and COV-ARCH, but only weakly represented in pfm9k.1b. The lack of a clear -0.25°/year signal in pfm9k.1b, compared to pfm9k.1a, shows how sensitive these observations are to age uncertainties in sedimentary data. In all three model families, there is also support for weaker eastward drift with similar rates.

## 4. Discussion

### *4.1 Potential sources for the detected high-latitude westward drift at the CMB*

We have shown, based on the pfm9k.1a model, that azimuthal motions at high northern latitudes of the CMB over the past 9000 years are dominated by westward drift concentrated to two distinct rates (-0.09°/year and -0.25°/year). While the slow drift rates have remained a persistent feature over most of the studied time interval, the faster drift rates appear to wax and wane with strong signals detected around 7000-6000 BC and during the last 3-4 millennia (see Fig. 1 and Fig. 2). We also find evidence for dominant strong westward drift (-0.22°/year) at high southern latitudes, but limitations with the model resolution prevents direct comparisons with the northern hemisphere observations. Comparisons between different models support the conclusions from pfm9k.1a but

also highlight how sensitive these observations are to the distribution and uncertainties of the data used to constrain the models. Based on these results we therefore restrict the following discussion to observations from the northern hemisphere and the past 3-4 millennia.

The observed drift is dominated by zonal wavenumbers $m$ = 2 and $m$ = 1. The $m$ = 2 signal essentially describes a slow westward motion of two intense high latitude flux patches, previously noted by Nilsson et al. (2014) for the past 4000 years. This could be interpreted as representing high latitude convection rolls (Gubbins and Bloxham, 1987) carried along by the mean zonal flow in the core. As shown in the TL plot in Figure 1, this pattern is only partly explained by continuous movement of individual flux patches and more generally generated by the appearance and disappearance of flux, e.g. migrating from lower or higher latitudes (or indeed from east or west). This would explain why similar patterns have gone largely unnoticed by other approaches designed to track the movements of individual flux patches (Amit *et al.*, 2011, Terra-Nova *et al.*, 2015, Terra-Nova *et al.*, 2016). Such discontinuities of flux movements at the CMB will likely arise as an effect of chronologic data uncertainties (Nilsson *et al.*, 2014), but it is perhaps also unlikely that individual flux patches remain intact/underformed over long timescales.

The observed $m$ = 1 drift rate is of the same magnitude as the classic westward drift (Bullard, 1950) and most likely the same signal as previously observed by Dumberry and Finlay (2007) and Hellio and Gillet (2018). The fact that the two detected drift rates shows a dispersive relationship (Figure 3a) indicates that one or both could, at least partially, be generated by magnetic Rossby waves. Such waves are expected to be mostly relevant at high latitudes as investigated here (Hori et al., 2015). However, the observed dispersion relation, with longer ($m$ = 1) wavelengths propagating with faster phase velocity, is opposite to the predicted dispersion for magnetic Rossby waves (Hide, 1966). One interpretation is that the $m$ = 1 signal represents a wave riding on the mean background flow, represented by the $m$ = 2 signal as suggested above. This would suggest a wave propagation speed of -0.16 °/year, after subtracting the background flow.

An alternative explanation may be provided by the forced magnetohydrodynamic waves proposed by Yoshida and Hamano (1993), which are expected to result in secular variation frequencies independent of zonal wavenumber. Such waves are hypothesised to be generated by variations in LOD that induce flow in the core due to topographic differences of the CMB. In their model, the frequency of the secular variation is the same as that of the external forcing, i.e. the variations in LOD. Interestingly, millennial-scale reconstructions of LOD based on historical records of solar and lunar eclipses (Morrison and Stephenson, 2001) show variations on similar timescales as the detected drift rates and have previously also been shown to correlate with changes in the dipole tilt (Nilsson et al., 2011).

*4.2 Wave interference and occurrence of high latitude weak/reverse flux*

As shown in Figure 3a, the observed westward drift at 60°N over the past 4000 years can largely be decomposed into two waveforms, represented by the two stars in the figure. To further examine the interference pattern predicted by the inferred waveforms we construct a simple model composed of two sinusoidal waves of the form

$$W(\phi, t) = \cos(m\phi - \omega t)$$

where $\phi$ = longitude, $t$ = time and $\omega = 2\pi f$ is the angular frequency of the waves (with angles given in radians). The superposition of the two waves gives rise to an interference pattern with an envelope wave propagating eastward with a group velocity $\left(v_g = \frac{\Delta\omega}{\Delta m}\right)$ of 0.07°/year. Constructive interference appears as an intensification of positive residual flux where the drift lines intersect in Figure 1. The time interval $t_c$ and longitudinal offset $\phi_c = v_g t_c$ between these points is calculated by setting $W(\phi_c, t_c) = 2\pi$ for one of the two inferred waveforms, which yields $t_c = 1125$ years and $\phi_c$ corresponding to 79°. The resultant interference pattern could be described as an eastward propagating beat frequency of 1/1125 years$^{-1}$.

When we compare this to the unfiltered radial field at 60°N at the CMB (Fig. 6a), we find that this interference pattern coincides, both in terms of timing and location, with the three high latitude weak/reverse flux patches previously noted by Nilsson et al. (2014). A similar pattern is also observed in other models (see supplementary information, Figures S3-S5), although the fine scale structure differs. To facilitate the comparisons, we have drawn yellow contour lines around what we (slightly arbitrarily) have defined as weak/reverse flux, weak flux corresponding to absolute $B_r$ below a certain threshold ($|B_r| \leq 0.25|B_r|_{MAX}$, where $|B_r|_{MAX}$ is defined over the whole CMB). As noted by Nilsson et al. (2014), the high latitude weak/reverse flux patches appear to originate from lower latitudes and migrate northwards. This suggests an important meridional component potentially related to something similar to the eccentric planetary-scale gyre observed in recent core-flow inversion (e.g. Pais and Jault, 2008, Gillet *et al.*, 2015)

To better quantify the occurrence of high latitude weak/reverse flux we calculated the area of the core at latitudes greater than 45°N covered by weak/reverse flux. The results, shown in Figure 6b, confirm that the occurrence of high latitude weak/reverse flux is generally consistent with the inferred 1125-year periodicity signal over the past three millennia, i.e. with maximum extents of 20-40% coinciding with the appearance of the three high latitude weak/reverse flux patches previously mentioned, followed by relatively quiet periods in between. We note that the maximum extents of weak/reverse flux are generally lower for the models based on palaeomagnetic data compared to *gufm1*. However, the results are consistent if we compare to *gufm1* truncated at spherical degree 5-

6, suggesting that the difference is due to the lower spatial resolution of the palaeomagnetic models (see Nilsson *et al.*, 2014).

### *4.3 Millennial-scale periodicity in the geomagnetic field*

A millennial-scale periodicity signal (~1350 year), similar to the 1125-year signal inferred from the interference pattern, has previously been identified in dipole tilt variations over the past 9000 years (Nilsson *et al.*, 2011, Korte *et al.*, 2011). Figure 6c shows that the changes in dipole tilt are mostly in phase with the predicted periodicity signal, with large tilt angles coinciding with occurrence of high latitude weak/reverse flux in the northern hemisphere. The agreement with the predicted periodicity signal becomes poorer the further back in time ones goes as the density of data decrease.

Interpretations of the observed westward drift in terms of high latitude convection rolls and/or magnetic Rossby waves imply a largely anti-symmetric field with respect to the equator. If these interpretations are correct, we may expect to find concentrations of weak or reverse field at high southern latitudes at similar times and longitudes where these are observed in the northern hemisphere (Fig 6a). This is consistent with the more or less anti-symmetric appearance and poleward migration of reverse flux patches in the Atlantic hemisphere associated with the development of the SAA, previously noted by Campuzano et al. (2019). In fact, the present field with SAA related to both high latitude reverse flux at the CMB and a strong equatorial dipole (Amit and Olson, 2008) might provide a good analogue of previous periods large dipole tilt over the past three millennia. However, while the growth of the SAA has been associated with a 9% drop in the axial dipole field, potentially driven by the poleward migration of the reverse flux (Finlay *et al.*, 2016, Gubbins, 1987), we do not see any similar changes in dipole field in current models during the proposed analogues in the past.

## 5. Conclusions

Through analyses on TL plots of the geomagnetic field model pfm9k.1a, filtered to remove quasi-stationary field structures, we have found evidence for persistent and dominant westward drift at high latitudes of the CMB over the past 9000 years. At high northern latitudes we identify two distinct drift rates of -0.09°/year and -0.25°/year with dominant zonal wavenumbers $m$ = 2 and $m$ = 1 respectively, both of which are present over the past 3-4 millennia. Comparisons with other geomagnetic field models that include sedimentary data show similar westward drift signals over the same time period. Constructive interference between two westward propagating waveforms, inferred from these observations, predicts the recurrence of high-latitude weak/reverse flux every ~1125 years with a longitudinal offset of approximately 80° to the east from the previous occurrence.

These predictions are largely in agreement with model observations over the same time period. In addition, the predicted 1125-year periodicity signal is positively correlated with variations in the dipole tilt over the past three millennia. We speculate that the two identified drift signals could be related to the westward motion of high latitude convection rolls and/or magnetic Rossby waves, originally proposed by Hide (1966). The detection of such waves in Earth's core could provide important constraints on the strength of the otherwise hidden toroidal part of the geomagnetic field (e.g. Hori et al., 2015). Improved model resolution at high northern and southern latitudes of the core would help to distinguish the proposed underlying processes, e.g. through further investigation into the dispersion relation, if a potential $m = 3$ signal can be resolved, and the proposed equatorial anti-symmetry of the detected signals.

## Acknowledgements

We would like to thank both Chris Finlay and Kumiko Hori for valuable discussions on the interpretation of our results as well as two anonymous reviewers whose comments considerably improved the manuscript. This work was partially funded by the Natural Environment Research Council, UK (grant number NE/I013873/1) and Swedish Research Council (grant number 2014–4125).

## References

Amit, H., Korte, M., Aubert, J., Constable, C. & Hulot, G., 2011. The time-dependence of intense archeomagnetic flux patches, *Journal of Geophysical Research: Solid Earth,* 116**,** B12106.

Amit, H. & Olson, P., 2008. Geomagnetic dipole tilt changes induced by core flow, *Phys. Earth Planet. Inter.,* 166**,** 226-238.

Arneitz, P., Egli, R., Leonhardt, R. & Fabian, K., 2019. A Bayesian iterative geomagnetic model with universal data input: Self-consistent spherical harmonic evolution for the geomagnetic field over the last 4000 years, *Phys. Earth Planet. Inter.,* 290**,** 57-75.

Aubert, J., Finlay, C.C. & Fournier, A., 2013. Bottom-up control of geomagnetic secular variation by the Earth/'s inner core, *Nature,* 502**,** 219-223.

Barletta, F., St-Onge, G., Channell, J.E.T., Rochon, A., Polyak, L. & Darby, D., 2008. High-resolution paleomagnetic secular variation and relative paleointensity records from the western Canadian Arctic: implication for Holocene stratigraphy and geomagnetic field behaviour, *Canadian Journal of Earth Sciences,* 45**,** 1265-1281.

Barrois, O., Hammer, M.D., Finlay, C.C., Martin, Y. & Gillet, N., 2018. Assimilation of ground and satellite magnetic measurements: inference of core surface magnetic and velocity field changes, *Geophys. J. Int.,* 215**,** 695-712.

Bloxham, J. & Gubbins, D., 1985. The secular variation of Earth's magnetic field, *Nature,* 317**,** 777-781.

Brown, M., Donadini, F., Nilsson, A., Panovska, S., Frank, U., Korhonen, K., Schuberth, M., Korte, M. & Constable, C., 2015. GEOMAGIA50.v3: 2. A new paleomagnetic database for lake and marine sediments, *Earth Planet Sp,* 67**,** 1-19.

Bullard, E.C., Freedman, C., Gellman, H. & Nixon, J., 1950. The Westward Drift of the Earth's Magnetic Field, *Philos. Trans. R. Soc. Lond. A,* 243**,** 67-92.

Campuzano, S., Gómez-Paccard, M., Pavón-Carrasco, F. & Osete, M., 2019. Emergence and evolution of the South Atlantic Anomaly revealed by the new paleomagnetic reconstruction SHAWQ2k, *Earth Planet. Sci. Lett.,* 512**,** 17-26.

Constable, C., Korte, M. & Panovska, S., 2016. Persistent high paleosecular variation activity in southern hemisphere for at least 10 000 years, *Earth Planet. Sci. Lett.,* 453**,** 78-86.

Dumberry, M. & Finlay, C.C., 2007. Eastward and westward drift of the Earth's magnetic field for the last three millennia, *Earth Planet. Sci. Lett.,* 254**,** 146-157.

Finlay, C.C., Aubert, J. & Gillet, N., 2016. Gyre-driven decay of the Earth/'s magnetic dipole, *Nat Commun,* 7.

Finlay, C.C., Dumberry, M., Chulliat, A. & Pais, M.A., 2010. Short Timescale Core Dynamics: Theory and Observations, *Space Sci. Rev.,* 155**,** 177-218.

Finlay, C.C. & Jackson, A., 2003. Equatorially Dominated Magnetic Field Change at the Surface of Earth's Core, *Science,* 300**,** 2084-2086.

Gillet, N., Jault, D. & Finlay, C.C., 2015. Planetary gyre, time-dependent eddies, torsional waves, and equatorial jets at the Earth's core surface, *Journal of Geophysical Research: Solid Earth,* 120**,** 3991-4013.

Gubbins, D., 1987. Mechanism for geomagnetic polarity reversals, *Nature,* 326**,** 167-169.

Gubbins, D. & Bloxham, J., 1987. Morphology of the geomagnetic field and implications for the geodynamo, *Nature,* 325**,** 509-511.

Halley, E., 1692. An account of the cause of the change of the variation of the magnetical needle. with an hypothesis of the structure of the internal parts of the earth: as it was proposed to the Royal Society in one of their late meetings, *Philosophical Transactions of the Royal Society of London,* 17**,** 563-578.

Hellio, G. & Gillet, N., 2018. Time-correlation-based regression of the geomagnetic field from archeological and sediment records, *Geophys. J. Int.,* 214**,** 1585-1607.

Hide, R., 1966. Free hydromagnetic oscillations of the earth's core and the theory of the geomagnetic secular variation, *Philos. Trans. R. Soc. Lond. A,* 259**,** 615-647.

Hori, K., Jones, C.A. & Teed, R.J., 2015. Slow magnetic Rossby waves in the Earth's core, *Geophys. Res. Lett.,* 42**,** 6622-6629.

458 Hori, K., Teed, R.J. & Jones, C.A., 2018. The dynamics of magnetic Rossby waves in spherical
459 dynamo simulations: A signature of strong-field dynamos?, *Phys. Earth Planet. Inter.,* 276**,**
460 68-85.
461 Korte, M., Constable, C., Donadini, F. & Holme, R., 2011. Reconstructing the Holocene
462 geomagnetic field, *Earth Planet. Sci. Lett.,* 312**,** 497-505.
463 Korte, M., Donadini, F. & Constable, C.G., 2009. Geomagnetic field for 0-3 ka: 2. A new series of
464 time-varying global models, *Geochem. Geophys. Geosyst.,* 10**,** Q06008,
465 doi:06010.01029/02008GC002297.
466 Korte, M., Genevey, A., Constable, C.G., Frank, U. & Schnepp, E., 2005. Continuous geomagnetic
467 field models for the past 7 millennia: 1. A new global data compilation, *Geochem. Geophys.*
468 *Geosyst.,* 6**,** Q02H15, doi:10.1029/2004GC000800.
469 Livermore, P.W., Hollerbach, R. & Finlay, C.C., 2017. An accelerating high-latitude jet in Earth's
470 core, *Nature Geosci.,* 10**,** 62-68.
471 Morrison, L.V., Stephenson, F.R., 2001. Historical eclipses and the variability of the Earth's
472 rotation. J. Geodyn. 32, 247-265.
473 Nilsson, A., Holme, R., Korte, M., Suttie, N. & Hill, M.J., 2014. Reconstructing Holocene
474 geomagnetic field variation: New methods, models and implications, *Geophys. J. Int.,* 198**,**
475 229-248, doi:210.1093/gji/ggu1120.
476 Nilsson, A., Muscheler, R. & Snowball, I., 2011. Millennial scale cyclicity in the geodynamo
477 inferred from a dipole tilt reconstruction, *Earth Planet. Sci. Lett.,* 311**,** 299-305.
478 Nilsson, A., Suttie, N. & Hill, M.J., 2018. Short-Term Magnetic Field Variations From the Post-
479 depositional Remanence of Lake Sediments, *Frontiers in Earth Science,* 6**,** doi:
480 10.3389/feart.2018.00039.
481 Pais, M.A. & Jault, D., 2008. Quasi-geostrophic flows responsible for the secular variation of the
482 Earth's magnetic field, *Geophys. J. Int.,* 173**,** 421-443.
483 Panovska, S., Korte, M., Finlay, C.C. & Constable, C.G., 2015. Limitations in paleomagnetic data
484 and modelling techniques and their impact on Holocene geomagnetic field models, *Geophys.*
485 *J. Int.,* 202**,** 402-418.
486 Pavón-Carrasco, F.J., Osete, M.L., Torta, J.M. & De Santis, A., 2014. A geomagnetic field model for
487 the Holocene based on archaeomagnetic and lava flow data, *Earth Planet. Sci. Lett.,* 388**,** 98-
488 109.
489 Terra-Nova, F., Amit, H., Hartmann, G.A. & Trindade, R.I.F., 2015. The time dependence of
490 reversed archeomagnetic flux patches, *Journal of Geophysical Research: Solid Earth,* 120**,**
491 2014JB011742.

492 Terra-Nova, F., Amit, H., Hartmann, G.A. & Trindade, R.I.F., 2016. Using archaeomagnetic field
493 models to constrain the physics of the core: robustness and preferred locations of reversed
494 flux patches, *Geophys. J. Int.,* 206**,** 1890-1913.
495 Wardinski, I. & Korte, M., 2008. The evolution of the core-surface flow over the last seven
496 thousands years, *Journal of Geophysical Research: Solid Earth,* 113**,** B05101.
497 Yoshida, S. & Hamano, Y., 1993. The westward drift of the geomagnetic field caused by length-of-
498 day variation, and the topography of the core-mantle boundary. *Geophysical Journal*
499 *International* 114, 696-710.

500

## Figures

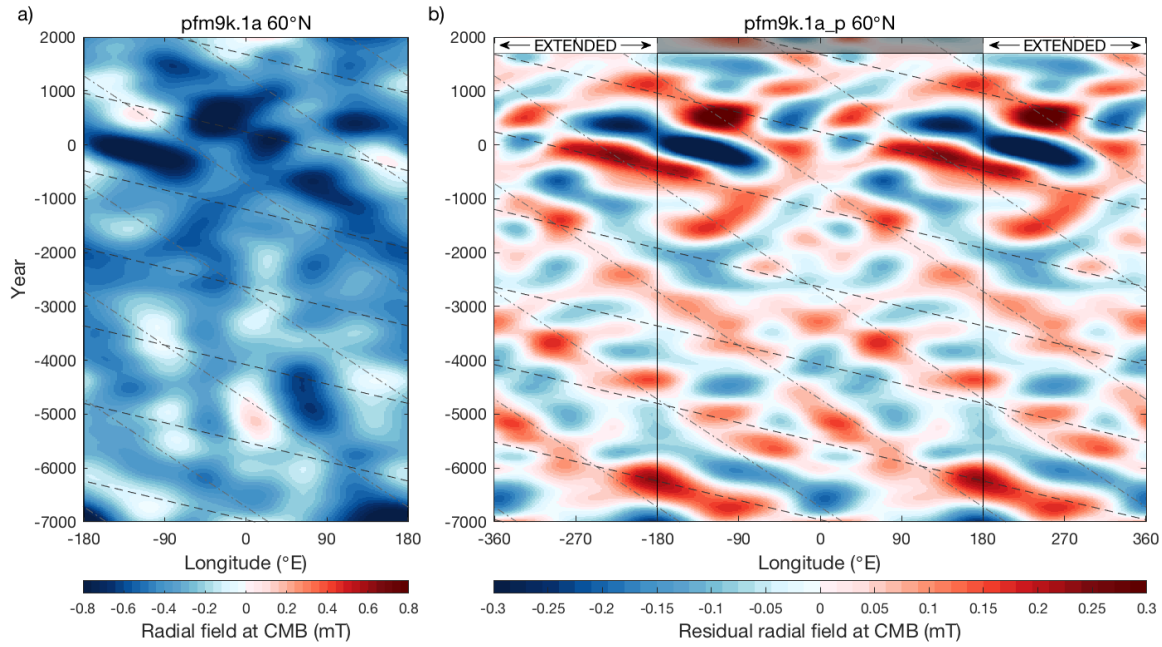


**Figure 1**: Time longitude (TL) plots (60°N) of the radial field at the core mantle boundary predicted by (a) pfm9k.1a and (b) pfm9k.1a_p, with the axisymmetric part of the field removed and high-pass filtered with cut-off frequency of 1/2500 $yr^{-1}$. The first and last 300 years of the filtered model were not considered during the analyses due to end-effects associated with the filtering process. Dot - dashed diagonal grey lines correspond to westward drift at rates of -0.09°/year ($f$ = -1/2000 $yr^{-1}$, $m$ = 2) and dashed grey lines correspond to drift rates of -0.25°/year ($f$ = -1/1440 $yr^{-1}$, $m$ = 1).

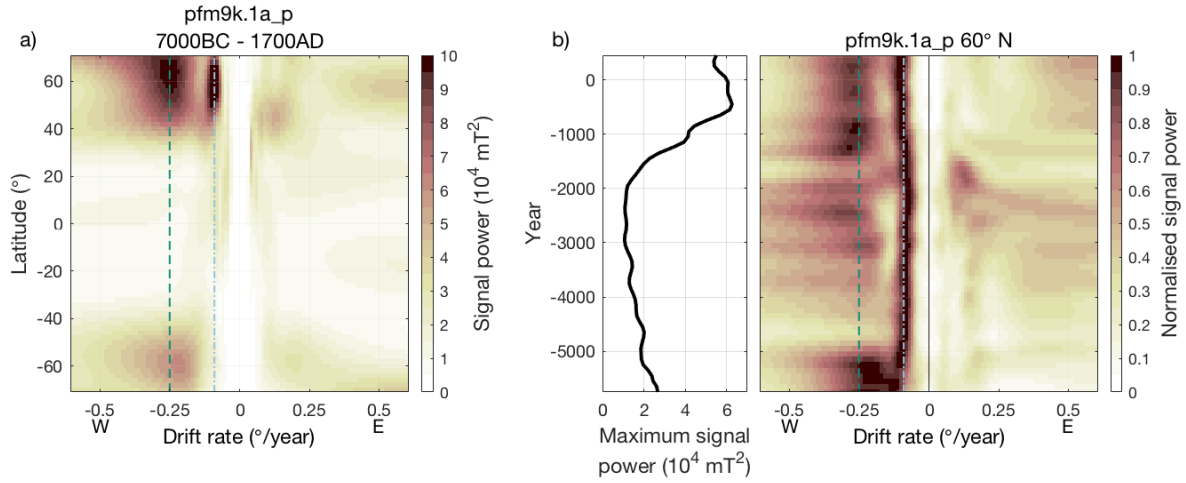


510

511 **Figure 2**: (a) Radon drift determination on time longitude (TL) plot of pfm9k.1a_p over the time
512 period 7000 BC to 1700 AD. The radon drift determination was performed for latitudes 70°S to 70°N
513 at 2° increments. The temporal and spatial resolution for each TL plot was 10 years and 2°. Vertical
514 green dashed and light blue dot-dashed lines denote westward rift rates of -0.25°/year and -
515 0.09°/year respectively. (b) Radon drift determination on TL plots of pfm9k.1a_p at 60°N over a
516 2500-year moving window (100 year increments). The signal power is normalised to the maximum
517 signal power (thick black line) in each time window. Vertical green dashed and light blue dot-dashed
518 lines denote westward rift rates of -0.25°/year and -0.09°/year respectively.

519

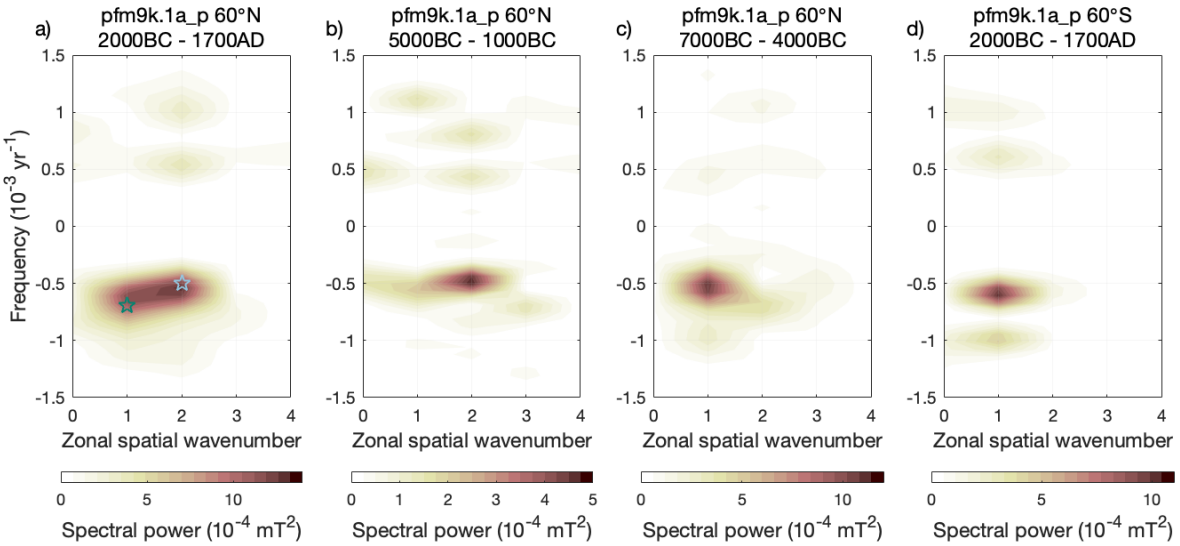


**Figure 3**: Frequency-wavenumber spectra of time-longitude plots based on pfm9k.1a_p at 60°N over time periods (a) 2000BC–1700AD, (b) 5000BC–1000BC, (c) 7000BC–4000BC and (d) at 60°S over 2000BC-1700AD. The light blue stars, frequency $f$ = -1/2000 yr$^{-1}$ and zonal wavenumber $m$ = 2, and green stars, frequency $f$ = -1/1440 yr$^{-1}$ and zonal wavenumber $m$ = 1, are shown for reference only. Positive (negative) frequencies indicate eastward (westward) drift.

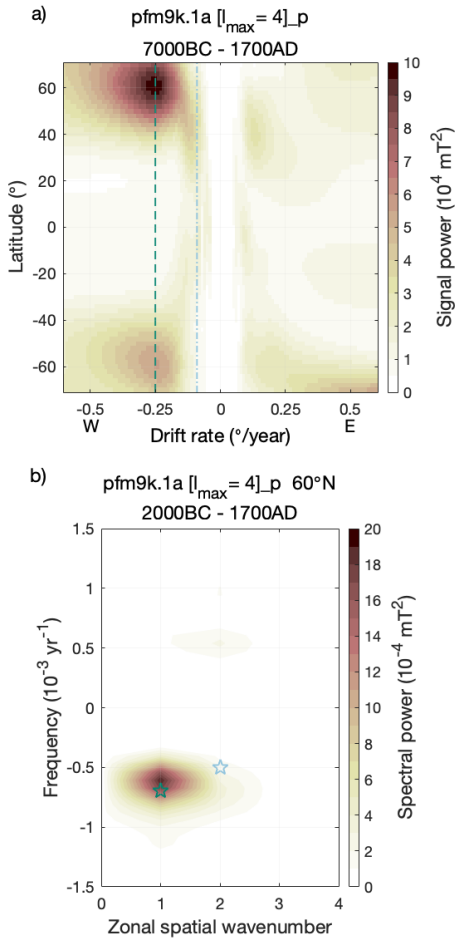


527

528 **Figure 4:** (a) Radon drift determination on time longitude (TL) plot of pfm9k.1a[$l_{max}$ = 4]_p (pfm9k.1a
529 truncated at spherical harmonic degree 4) over the time period 7000 BC to 1700 AD. The radon drift
530 determination was performed for latitudes 70°S to 70°N at 2° increments. The temporal and spatial
531 resolution for each TL plot was 10 years and 2°. Vertical green dashed and light blue dot-dashed lines
532 denote westward rift rates of -0.25°/year and -0.09°/year respectively. (b) Frequency-wavenumber
533 spectra of time-longitude plots over the time period 2000BC–1700AD at 60°N based on pfm9k.1a[$l_{max}$
534 = 4]_p. The light blue stars, frequency $f$ = -1/2000 $yr^{-1}$ and zonal wavenumber $m$ = 2, and green stars,
535 frequency $f$ = -1/1440 $yr^{-1}$ and zonal wavenumber $m$ = 1, are shown for reference only. Positive
536 (negative) frequencies indicate eastward (westward) drift.

537

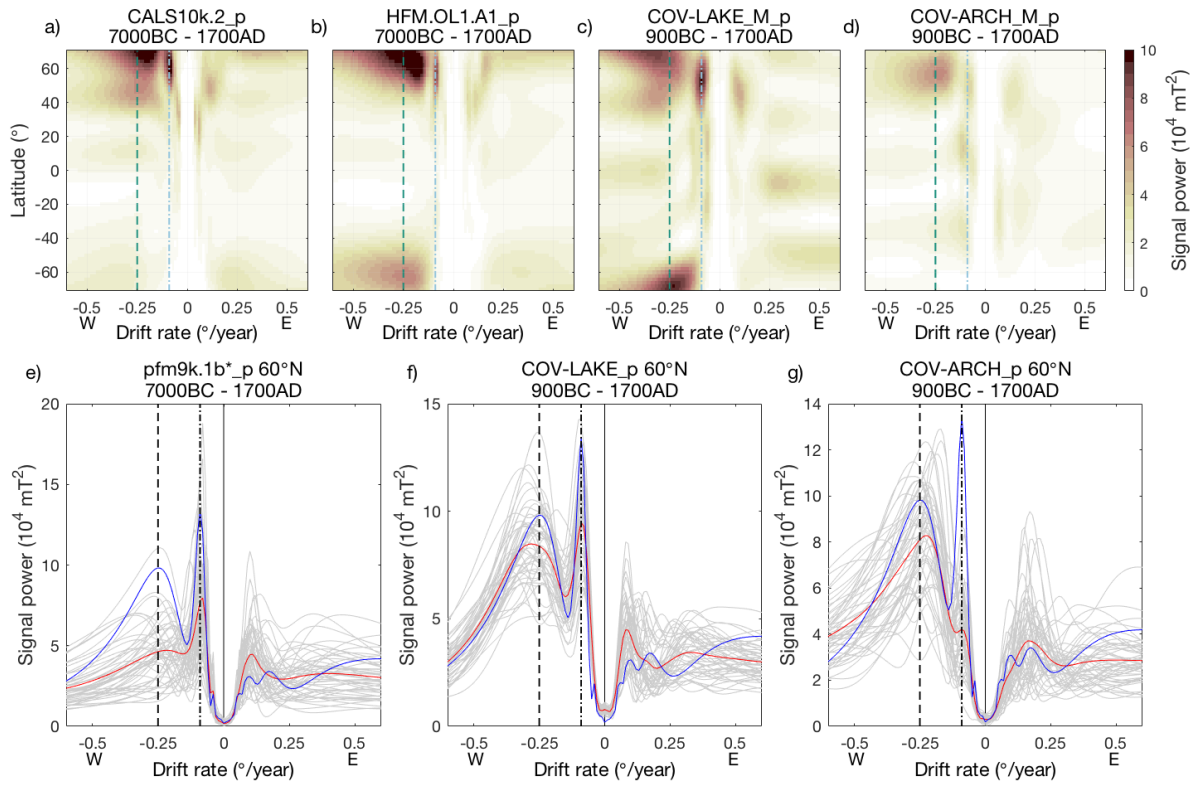


**Figure 5**: (upper panel) Model comparison of Radon drift determinations on time longitude (TL) plot of (a) CALS10k.2_p and (b) HFM.OL1.A1_p over the time period 7000 BC to 1700 AD and of (c) COV-LAKE_M_p and (d) COV-ARCH_M_p over the time period 900 BC to 1700 AD. The suffix 'M' indicates that it is the mean model from an ensemble. All drift determinations were performed for latitudes 70°S to 70°N at 2° increments. The temporal and spatial resolution for each TL plot was 10 years and 2°. Vertical green dashed and light blue dot-dashed lines denote westward rift rates of -0.25°/year and -0.09°/year respectively. (lower panel) Comparison of Radon drift determinations at 60°N between 50 randomly selected models (grey lines) from the same ensembles; (e) pfm9k.1b_p, (f) COV-LAKE_p and (g) COV-ARCH_p. The average signal (red line) and the drift determination of pfm9k.1a_p (blue line) are shown for reference. Vertical light blue dot-dashed and green dashed lines denote westward rift rates of -0.09°/year and -0.25°/year respectively.

* For a more informative comparison the individual pfm9k.1b bootstrap models were remade using the same temporal damping that was used for pfm9k.1a, chosen to smooth out variations on timescales shorter than 300-400 years (see Nilsson et al., 2014).

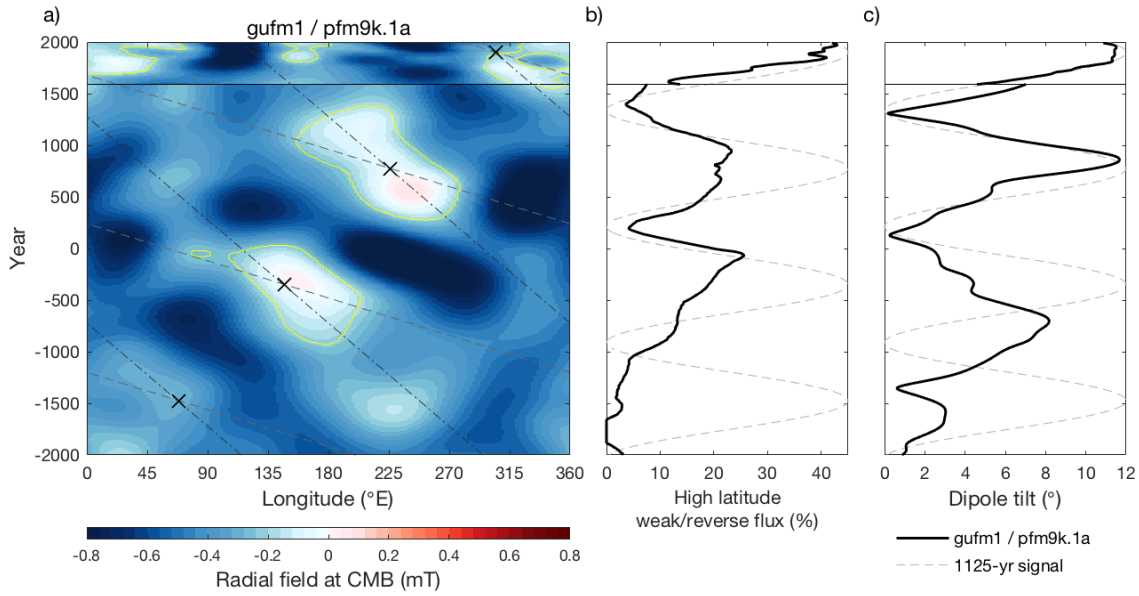


554

555 **Figure 6**: Time-longitude (TL) plots at 60°N of radial field at the core mantle boundary predicted by
556 (a) *gufm1* (1590 – 1990 AD) and pfm9k.1a (2000 BC – 1590 AD). Solid yellow lines denote areas with
557 weak/reverse flux (for details see main text). Dot-dashed diagonal grey lines correspond to westward
558 drift at rates of -0.09°/year ($f$ = -1/2000 yr$^{-1}$, $m$ = 2), dashed grey lines correspond to drift rates of -
559 0.25°/year ($f$ = -1/1440 yr$^{-1}$, $m$ = 1) and black crosses mark the time and longitude of constructive
560 interference between the two waveforms. Model comparison of (b) High latitude weak/reverse flux
561 occurrence calculated as the area of the core above 45°N latitude covered by weak/reverse flux (see
562 main text for details), (c) dipole tilt variations. The dashed grey lines (b-c) shows the 1125-periodicity
563 signal (arbitrarily scaled amplitude) resulting from the interference pattern of inferred waveforms
564 with peak values coinciding with crosses in (a).